Available on the CERN CDS information server **CMS PAS B2G-15-008**

CMS Physics Analysis Summary

Contact: cms-pag-conveners-b2g@cern.ch 2016/04/01

Search for Single Production of a Heavy Vector-Like Top Quark Partner Decaying to a Higgs Boson and a Leptonically Decaying Top Quark

The CMS Collaboration

Abstract

We search for singly produced vector-like top quark partners (T) in pp collisions at a center-of-mass energy of 13 TeV with the CMS experiment at the LHC. This is of particular interest, as the rate of single production of TeV-scale vector-like quarks increases faster than the rate of pair production with increasing centre-of-mass energy. The decay of a vector-like T quark into a Higgs boson and a top quark is searched for. The top quark decay includes an electron or a muon and the Higgs boson decays into a pair of b quarks. No significant excess over standard model backgrounds is observed. Exclusion limits on the production cross section times branching fraction, as well as exclusion limits on T quark coupling parameters are derived in the mass-range of 700 GeV to 1800 GeV. For a mass of 1000 GeV, we exclude production cross section times branching fractions above 0.9 pb and 0.6 pb at 95% confidence level, assuming left and right handed coupling of the T quark to standard model particles, respectively.

1 Introduction

Over the past decades several theories have been formulated that try to give new insights into electroweak symmetry breaking and the mechanisms that stabilise the mass of the Higgs boson. Several of these theories predict the existence of heavy vector-like quarks. Examples are little Higgs models [1, 2], models with extra dimensions [3, 4], and composite Higgs models [3–5].

The distinctive property of vector-like quarks is that their left-handed and right-handed components transform in the same way under the standard model (SM) electroweak symmetry group $\mathrm{SU}(2)_\mathrm{L} \times \mathrm{U}(1)_\mathrm{Y}$. As a consequence vector-like quarks can obtain mass through direct mass terms in the Lagrangian of the form $m\overline{\psi}\psi$, unlike the SM chiral quarks that obtain mass through a Yukawa coupling.

The discovery of a Higgs boson by the ATLAS [6] and CMS [7, 8] collaborations and the electroweak fits within the framework of the SM [9], strongly disfavour the existence a fourth generation of chiral fermions. Given the modest impact that vector-like quarks have on the properties of the SM Higgs boson, they are not similarly constrained [10].

This paper presents the results of a search for vector-like T quarks with charge $2/3\,e$. Many of the models mentioned above predict that the T quark will dominantly decay to third generation SM quarks in three decay modes: tH, tZ, and bW [10]. Searches for T quarks have been performed by the CMS and ATLAS collaborations setting lower limits on the T quark mass ranging from 715 to 950 GeV for different T quark branching fractions [11–14].

While these searches generally considered pair production of the T quarks via the strong interaction, we target the single production mode where the T quark is produced through the weak interaction. There are no a priori constraints on the T quark coupling to electroweak bosons. Therefore, not only the general coupling to the electroweak sector but couplings of the T quark to bW, tZ and tH can also take arbitrary values. The presented analysis is optimised for decays of the T quark into a Higgs boson and a top quark. It will be sensitive to the discovery of a T quark only if sufficiently large couplings to both, bW (tZ) and tH, exist in nature. An example of a Feynman diagram for this process is shown in Fig. 1.

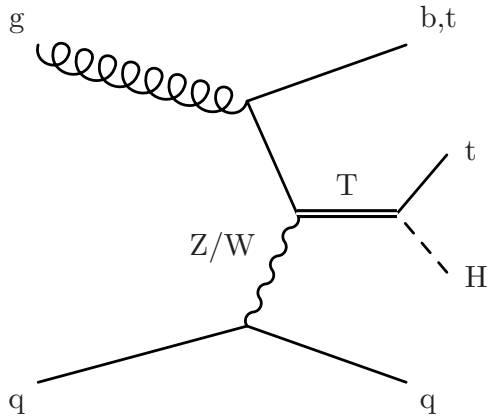

Figure 1: Production and decay mechanisms of a vector-like top quark partner, as targeted in this analysis.

The analysis is performed on the proton-proton collision data collected during 2015 by the CMS experiment at the CERN LHC at a centre-of-mass energy of $\sqrt{s}$=13 TeV. The search targets decays of the T quark into a Higgs boson and a leptonically decaying top quark. The Higgs boson is required to decay further into b quarks, as this is the Higgs boson final state with the largest branching fraction. For sufficiently large T quark masses, the decay products can be

highly Lorentz-boosted leading to merged jets and non-isolated leptons in the final state. Jet substructure analysis in combination with algorithms for the identification of b quark jets (b tagging) has proved to be an extremely powerful analysis tool for identifying boosted decays of the Higgs boson into b quark pairs, as shown in [15]. An additional distinctive feature of the signal is the presence of a jet in the forward region of the detector. The forward jet results from the light flavour quark that is produced in association with the vector-like T quark.

The top quark pair background is dominant, followed by W+jets and QCD multijet processes. While QCD multijet events can be suppressed using kinematic properties and isolation of the lepton with the highest p_T, a robust evaluation of the $t\bar{t}$ and W+jets event yield is provided by a background estimate that we take from the recorded data.

In the following, we briefly describe the CMS detector in Section 2. Section 3 describes the data and the simulated samples. Section 4 describes the objects employed in the event selection, which is outlined in Section 5. The estimate of the SM backgrounds is treated in Section 6. Section 7 describes the treatment of systematic uncertainties and the final results are presented in Section 8.

2 The CMS Detector

The central feature of the CMS apparatus is a superconducting solenoid of 6 m internal diameter, providing a magnetic field of 3.8 T. Within the superconducting solenoid volume are a silicon pixel and strip tracker, a lead tungstate crystal electromagnetic calorimeter (ECAL), and a brass-scintillator hadron calorimeter (HCAL), each composed of a barrel and two endcap sections. Forward calorimeters extend the pseudorapidity [16] coverage provided by the barrel and endcap detectors. Muons are measured in gas-ionisation detectors embedded in the steel flux-return yoke outside the solenoid.

A particle-flow algorithm is used to reconstruct and identify each individual particle in an event with an optimised combination of information from the various elements of the CMS detector [17, 18]. The energy of photons is directly obtained from the ECAL measurement, corrected for zero-suppression effects. The energy of electrons is determined from a combination of the electron momentum at the primary interaction vertex as determined by the tracker, the energy of the corresponding ECAL cluster, and the energy sum of all bremsstrahlung photons spatially compatible with originating from the electron track. The momentum resolution for electrons with $p_T \approx 45$ GeV from $Z \to ee$ decays ranges from 1.7% for nonshowering electrons in the barrel region to 4.5% for showering electrons in the endcaps [19]. Muons are measured in the pseudorapidity range $|\eta| < 2.4$ with detection planes made using three technologies: drift tubes, cathode strip chambers, and resistive plate chambers. Matching muons to tracks measured in the silicon tracker results in a relative transverse momentum resolution for muons with $20 < p_T < 100$ GeV of 1.3—2.0% in the barrel and better than 6% in the endcaps. The p_T resolution in the barrel is better than 10% for muons with p_T up to 1 TeV [20]. The energy of charged hadrons is determined from a combination of their momenta measured in the tracker and the matching ECAL and HCAL energy deposits, corrected for zero-suppression effects and for the response function of the calorimeters to hadronic showers. Finally, the energy of neutral hadrons is obtained from the corresponding corrected ECAL and HCAL energy.

Jets are reconstructed from the individual particles produced by the particle-flow event algorithm, clustered by the anti-k_t algorithm [21, 22] with a size parameter of 0.4 ('jets') and 0.8 ('AK8 jets'). Jet momentum is determined as the vectorial sum of all particle momenta in the jet that are identified as originating from the primary interaction vertex or that are not asso-

ciated to a primary vertex. It is found from simulation to be within 5—10% of the true jet momentum over the whole p_T spectrum and detector acceptance. An area based correction is applied to jet energies to take into account the contribution from additional proton-proton interactions within the same bunch crossing [23]. Jet energy corrections are derived from simulation, and are confirmed with in situ measurements of the energy balance in dijet and photon+jet events [24]. A smearing of the jet energy is applied to simulated events to mimic detector resolution effects observed in data. Additional selection criteria are applied to each event to remove spurious jet-like features originating from isolated noise patterns in certain HCAL regions. The jet energy resolution is typically 15% at 10 GeV, 8% at 100 GeV, and 4% at 1 TeV.

The missing transverse momentum vector $\vec{p}_T^{\,\text{miss}}$ is defined as the projection on the plane perpendicular to the beams of the negative vector sum of the momenta of all reconstructed particles in an event. Its magnitude is referred to as E_T^{miss}.

A more detailed description of the CMS detector, together with a definition of the coordinate system used and the relevant kinematic variables, can be found in Ref. [16].

3 Samples

Events in the muon channel are collected with a single-muon trigger, requiring the presence of a muon with $p_T > 45\,\text{GeV}$ and $|\eta| < 2.1$. Events in the electron channel are selected using an electron trigger which requires an electron with $p_T > 45\,\text{GeV}$ and the additional presence of at least two jets, with thresholds of $p_T > 200\,\text{GeV}$ and $p_T > 50\,\text{GeV}$ respectively for the jets with the highest and second highest p_T. Neither of the triggers places any requirement on the isolation of the leptons. If an event is selected by both triggers, it is assigned to the muon channel. The data collected with the muon trigger correspond to a luminosity of $\mathcal{L} = 2.3\,\text{fb}^{-1}$, while the electron trigger provides a luminosity of $\mathcal{L} = 2.2\,\text{fb}^{-1}$. The data are filtered to remove events originating from detector noise or beam backgrounds, and events that were collected when the detector was not optimally operated.

Top quark pair events are simulated with the next-to-leading-order generator POWHEG v2 [25–28], which is also used for the electroweak production of single top quarks in the tW channel [29]. The AMC@NLO v5.2.2.2 generator is used for the s- and t-channel processes of single top quark production [30]. The generation of the W+jets and Z+jets backgrounds was performed with MADGRAPH v5.2.2.2 [30]. The MLM matching scheme is used, allowing up to four additional partons in the matrix element [31]. All samples are interfaced to PYTHIA 8.212 for the showering [32, 33]. The QCD multijet background is generated with PYTHIA both for matrix element and showering.

Signal samples are generated using MADGRAPH interfaced to PYTHIA for T quark mass hypotheses between 700 and 1800 GeV in steps of 100 GeV. A width of 10 GeV is used for all mass points. Both charge conjugates are included by the generator, where the T quark with positive charge has a higher occurrence because of the larger density of positively charged partons in the proton. Left-handed and right-handed coupling of the T quark to the SM particles are treated separately.

All events are generated using the parton distribution functions (PDF) from the NNPDF 3.0 PDF sets [34], while for the showering the underlying event tune CUETP8M1 is used. The presence of additional collisions contributing both from within the same beam crossing (in-time pileup) as well as from the previous and following bunch crossings (out-of-time pileup) is simulated in all samples.

4 Physics object definitions

Primary vertices are reconstructed using a deterministic annealing filtering algorithm [35]. The leading vertex of the primary interaction of the event is defined as the vertex with the largest summed square of transverse momenta of associated tracks. Its position is reconstructed using an adaptive vertex fit [36] and is required to be within 24 cm in the z-direction and less than 2 cm in the x-y plane away from the nominal interaction point. In order to match the simulated pileup to the observed distribution in data, simulated events are reweighted assuming a minimum-bias cross-section of 69 mb.

In signal events, the top quark from the T quark decay will have a large Lorentz boost. The top quark decay products will therefore be approximately collinear and the lepton will not be isolated from the b jet. Thus, no conventional isolation requirement (that the amount of energy deposits in a cone around the lepton is small) is applied. In order to suppress QCD multijet events with a soft lepton contained within a jet, we require that $\Delta R(\ell, j) > 0.4$ or $p_T^{\text{rel}}(\ell, j) > 40\,\text{GeV}$, where ℓ indicates the lepton and j indicates the jet with closest angular separation from the lepton. The angular distance is defined as $\Delta R = \sqrt{\Delta\eta^2 + \Delta\phi^2}$ and p_T^{rel} is the projection of the 3-momentum of the lepton onto a plane perpendicular to the jet axis. In addition to this selection, electrons must have $p_{\text{T}} > 50\,\text{GeV}$ and $|\eta| < 2.5$, while muons are required to have $p_{\text{T}} > 47\,\text{GeV}$ and $|\eta| < 2.1$, to operate in a region where the trigger efficiency is constant. In case of more than one reconstructed lepton, only the lepton with the highest p_{T} is used in the evaluation of physics quantities and in the figures shown in the following. The efficiency of the muon identification and trigger selection in the simulation is corrected depending on η and p_{T} of the muon in order the match the efficiencies found in the data. For the electron, such corrections are found to be negligible within their uncertainty.

All jets are required to have $p_{\text{T}} > 30\,\text{GeV}$. Jets with $|\eta| > 2.4$ are defined as 'forward' jets. Large-cone AK8 jets are required to have $p_{\text{T}} > 200\,\text{GeV}$ and $|\eta| > 2.4$. In order to resolve ambiguities, if a lepton is found within a cone of $\Delta R(j, \ell) < 0.4$ around the jet axis, the lepton four-vector is subtracted from the uncorrected jet four-vector and all jet energy corrections are applied thereafter.

For the identification of b jets the combined secondary vertex (CSV) algorithm is used [37]. A loose selection is used, which yields typical b tagging efficiencies of approximately 80% and misidentification rates from light flavour jets of about 10% in $\text{t}\bar{\text{t}}$ events [37]. The CSV algorithm is not applied to jets, but to subjets of AK8 jets, in order to identify boosted decays of the Higgs boson to b quark pairs (H tagging) [15]. The subjets of AK8 jets are identified using a soft-drop algorithm [38]. We require both soft-drop subjects to be b-tagged and the soft-drop mass of the jet, $M_{\text{H,rec}}$, to be within $90\,\text{GeV} < M_{\text{H,rec}} < 160\,\text{GeV}$. The soft-drop jet mass scale and resolution have been estimated in a $\text{t}\bar{\text{t}}$ control region and are found to be compatible within uncertainties. A smearing of the jet mass resolution is applied in the simulation to match the resolution found in the data. The observable S_{T} is defined as the scalar sum over $E_{\text{T}}^{\text{miss}}$, the p_{T} of the lepton, and the p_{T} of all reconstructed jets in the event.

5 Event Reconstruction and Selection

Events are required to have at least one lepton reconstructed offline, fulfilling the criteria discussed above, and two central jets. The jet with highest (second-highest) p_{T} is required to have $p_{\text{T}} > 250\,\text{GeV}$ ($> 70\,\text{GeV}$) in the electron channel and $p_{\text{T}} > 100\,\text{GeV}$ ($> 50\,\text{GeV}$) in the muon channel. The different p_{T} thresholds for the two channels are due to the tighter criteria of the electron trigger, which selects events with two high-p_{T} jets (Sec. 3). Additionally, we require

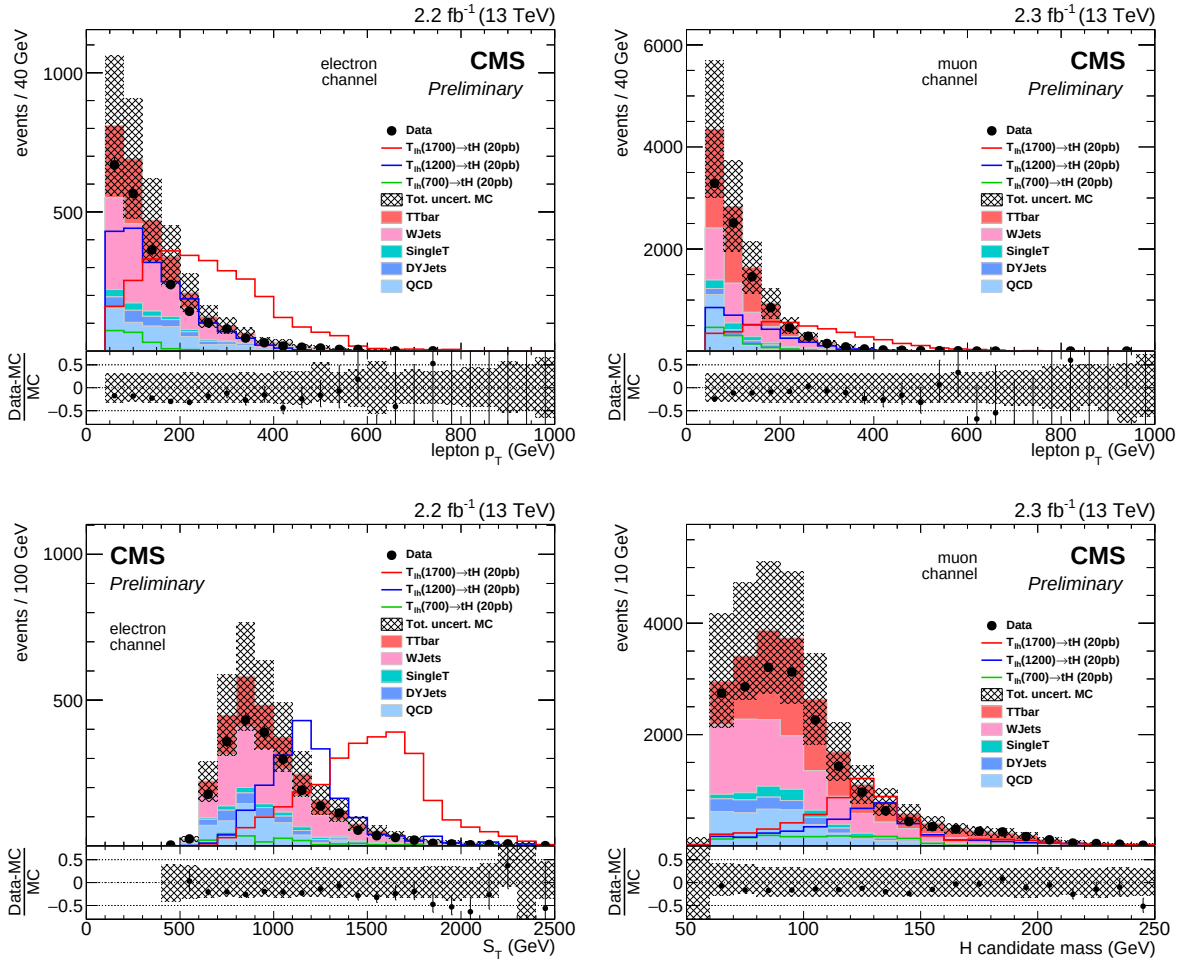

Figure 2: Distributions of physics object quantities after the 'baseline' event selection (see Sec. 5). Electron and muon p_{T} distributions are depicted in the top left and right graphs. The lower left shows S_{T} in the electron channel and the soft-drop mass of the Higgs boson candidate in the muon channel is depicted in the lower right.

$S_T > 400\,\text{GeV}$ and at least one Higgs boson candidate. The Higgs boson candidate is required to have an angular separation from the lepton of $\Delta R(j,l) > 1.0$.

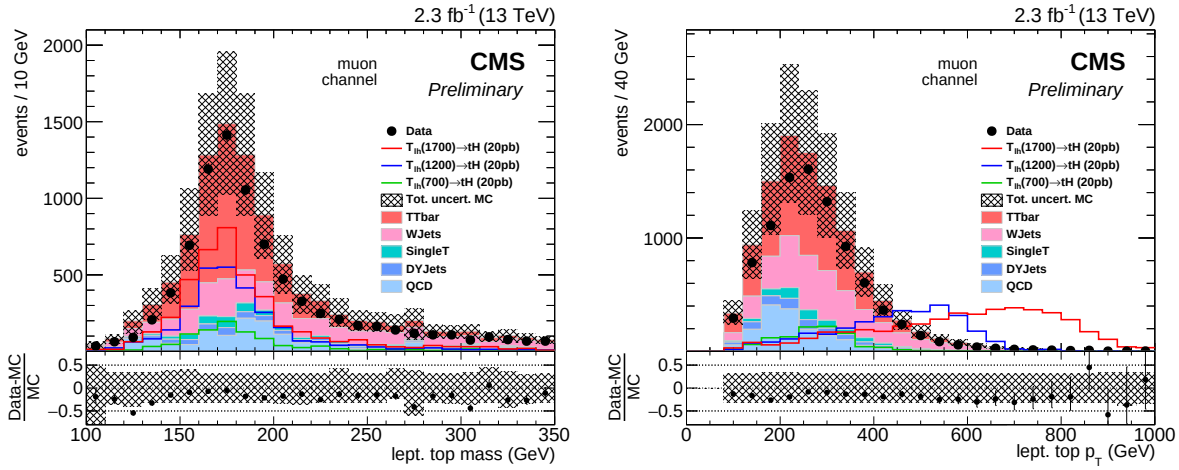

Figure 3: Mass and p_T distributions of the reconstructed top quark candidate in the muon channel on the left and right side, respectively. The 'baseline' event selection is applied.

For every event, we attempt to construct the mass of the T quark from all possible reconstruction hypotheses consistent with the identification of the top quark and Higgs boson candidates. To reconstruct the top quark we attempt to identify its decay into a b quark and a W, which decays leptonically into a muon or electron and a neutrino. Using the x- and y-components of E_T^{miss}, the lepton four-vector and the nominal mass of the W boson, $M_W = 80.4\,\text{GeV}$, the z-component of the neutrino momentum is reconstructed by solving a quadratic equation, yielding up to two solutions. If imaginary solutions are obtained, only the real part is used. Combining the four-momenta of these neutrino hypotheses and the lepton, up to two W boson candidates are obtained. Each W boson candidate is paired to every central jet in the event, giving a range of reconstruction hypotheses for the top quark. In order to accommodate final state radiation from the top quark, many more top quark reconstruction hypotheses are found by the addition of one more jet, where all possible combinations of two central jets are established. Out of all combinations of top quark hypotheses and Higgs boson candidates, the one yielding the smallest χ^2 value is picked, where the χ^2 function is defined as follows:

$$\chi^2 = \left(\frac{M_{\text{H,MC}} - M_{\text{H,rec}}}{\sigma_{\text{M}_\text{H},\text{MC}}}\right)^2 + \left(\frac{M_{\text{t,MC}} - M_{\text{t,rec}}}{\sigma_{\text{M}_\text{t},\text{MC}}}\right)^2 + \left(\frac{\Delta R(\text{t},\text{H})_{\text{MC}} - \Delta R(\text{t},\text{H})_{\text{rec}}}{\sigma_{\Delta R,\text{MC}}}\right)^2$$

where M denotes the mass of a candidate, and the H and t subscripts stand for Higgs boson and top quark candidates, respectively. The "MC" subscript denotes that a quantity is derived from a signal sample with the T quark mass of 1200 GeV, using the correct pairing of the reconstructed objects based on Monte Carlo information. A quantity with a "rec" subscript is obtained from the reconstruction hypotheses. Combinations are rejected if any jet of the top quark hypothesis overlaps with the Higgs Boson candidate within $\Delta R(j_t, H) < 1.0$.

After the event reconstruction the selection is further refined by requiring a large angular separation of $\Delta R(t,H) > 2$ between the top quark and Higgs boson candidates. The top quark candidate must have $p_{T,t} > 100\,\text{GeV}$. This selection is referred to as the 'baseline' selection. Relevant physics quantities are shown in Figs. 2 and 3. The T quark candidate momentum is obtained from the sum of the Higgs boson and the top quark candidate four-vectors, choosing the hypothesis with smallest χ^2. The T quark mass, M^T, is used as the discriminating variable

in the limit setting procedure.

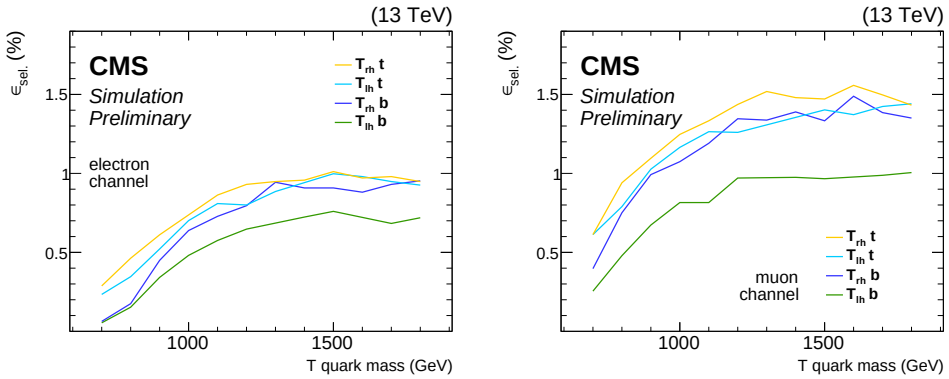

Figure 4: Selection efficiency for the signal samples. The denominator of the efficiency includes all decay modes of the top quark and the Higgs boson. On the left hand side, the electron channel is depicted, the muon channel is shown on the right. Left (right) handed coupling of the T quark to standard model particles is denoted by a lh (rh) subscript.

The baseline selection is used as a basis to define a signal region and statistically independent background control regions. The background control regions are signal-depleted and used for the background estimation in the signal region, as discussed in Sec. 6.

The signal region is obtained by additionally requiring that both soft-drop subjets of the Higgs boson candidate are b tagged and that there is at least one forward jet. In the signal region, we select 35 data events in the electron channel and 134 events in the muon channel, as summarised in Tab. 1 along with the event yields and selection efficiencies for three of the signal samples. The signal selection efficiency is also depicted in Fig. 4. Fig. 5 shows the predicted background composition and signal shapes.

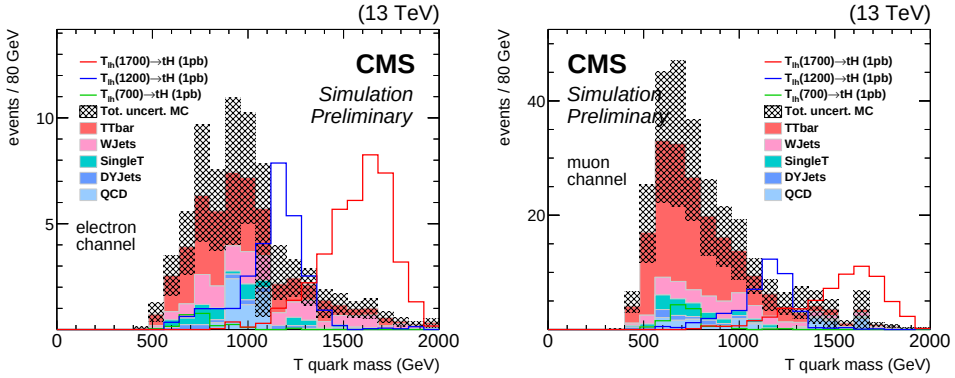

Figure 5: Vector-like T quark mass in the signal region. The electron channel is depicted on the left side and the muon channel on the right side.

6 Background estimate

The combined shape of all background processes in the signal region is estimated by the data in a 'sideband region'. Given the background shape, its yield is constrained through a fit of a signal plus background model to the data distribution in the signal region that will be detailed in Sec. 8. The sideband region is defined by requiring the absence of forward jets and that exactly one of the soft-drop subjets of the Higgs boson candidates is b tagged. The event selection criteria for both the signal and sideband regions are summarised in Tab. 2.

Table 1: Selection efficiency and number of selected events for the signal region. For the background, we quote the post-fit value as determined by the fit (see Sec. 6 and 8). The left (right) handed T quark coupling to standard model particles is denoted by a lh (rh) subscript. T quark production in association with a bottom quark (b) is given in the first six table rows, and the associated production with a top quark (t) in the next six rows. All signal samples are normalised to a cross section of 1 pb and include all decay modes of the top quark and the Higgs boson.

	electron channel		muon channel	
	$N_{\text{sel}} \pm \text{stat} \pm \text{sys}$	$\epsilon_{\text{sel}} \pm \text{stat} \pm \text{sys}$ (%)	$N_{\text{sel}} \pm \text{stat} \pm \text{sys}$	$\epsilon_{\text{sel}} \pm \text{stat} \pm \text{sys}$ (%)
$T_{lh}(700)$ b	$1.0 \pm 0.2 \pm 0.4$	$0.04 \pm 0.01 \pm 0.02$	$5.9 \pm 0.6 \pm 0.9$	$0.25 \pm 0.03 \pm 0.04$
$T_{lh}(1200)$ b	$13.7 \pm 0.8 \pm 1.6$	$0.62 \pm 0.04 \pm 0.07$	$22.4 \pm 1.1 \pm 2.7$	$0.97 \pm 0.05 \pm 0.12$
$T_{lh}(1700)$ b	$14.9 \pm 0.9 \pm 2.0$	$0.67 \pm 0.04 \pm 0.09$	$22.1 \pm 1.1 \pm 2.3$	$0.95 \pm 0.05 \pm 0.10$
$T_{rh}(700)$ b	$1.3 \pm 0.3 \pm 0.5$	$0.06 \pm 0.01 \pm 0.02$	$8.6 \pm 0.7 \pm 1.6$	$0.37 \pm 0.03 \pm 0.07$
$T_{rh}(1200)$ b	$17.3 \pm 0.9 \pm 2.1$	$0.78 \pm 0.04 \pm 0.09$	$29.9 \pm 1.3 \pm 3.5$	$1.29 \pm 0.06 \pm 0.15$
$T_{rh}(1700)$ b	$20.2 \pm 1.0 \pm 2.3$	$0.91 \pm 0.04 \pm 0.10$	$31.4 \pm 1.3 \pm 2.9$	$1.35 \pm 0.06 \pm 0.13$
$T_{lh}(700)$ t	$5.1 \pm 0.5 \pm 0.8$	$0.23 \pm 0.02 \pm 0.04$	$13.8 \pm 0.9 \pm 2.0$	$0.60 \pm 0.04 \pm 0.09$
$T_{lh}(1200)$ t	$16.8 \pm 0.9 \pm 1.8$	$0.76 \pm 0.04 \pm 0.08$	$29.1 \pm 1.2 \pm 3.1$	$1.26 \pm 0.05 \pm 0.13$
$T_{lh}(1700)$ t	$20.5 \pm 1.0 \pm 1.9$	$0.92 \pm 0.04 \pm 0.09$	$32.4 \pm 1.3 \pm 3.0$	$1.40 \pm 0.06 \pm 0.13$
$T_{rh}(700)$ t	$6.4 \pm 0.6 \pm 1.1$	$0.29 \pm 0.03 \pm 0.05$	$14.2 \pm 0.9 \pm 1.6$	$0.61 \pm 0.04 \pm 0.07$
$T_{rh}(1200)$ t	$19.5 \pm 1.0 \pm 2.0$	$0.88 \pm 0.04 \pm 0.09$	$32.6 \pm 1.3 \pm 2.6$	$1.41 \pm 0.06 \pm 0.11$
$T_{rh}(1700)$ t	$21.2 \pm 1.0 \pm 2.1$	$0.95 \pm 0.04 \pm 0.09$	$33.5 \pm 1.4 \pm 2.9$	$1.45 \pm 0.06 \pm 0.13$
bkg (post-fit)	34.8 ± 1.4		133.4 ± 2.5	
Data	35		134	

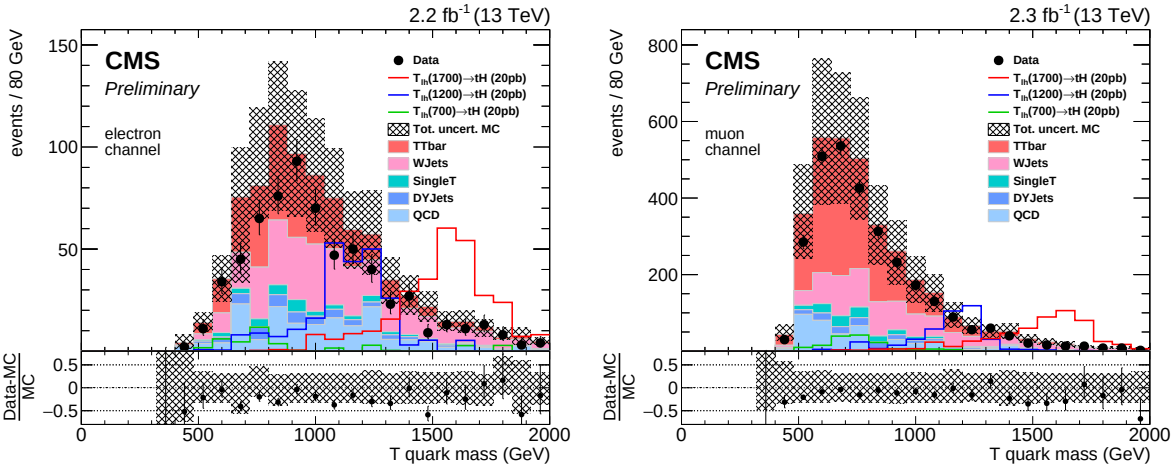

Figure 6: Vector-like T quark mass in the sideband region. The shape information encoded in the data histogram constitutes the background estimate. The electron channel is depicted on the left side and the muon channel on the right side.

Table 2: Event selection criteria for the signal and sideband regions.

region	signal	sideband
number of subjet b-tags (H cand.)	exactly 2	exactly 1
number of forward jets	at least 1	exactly 0

Fig. 6 shows the reconstructed mass of the T quark candidates in the sideband region, where good MC-to-data shape agreement is achieved. The sideband region features a signal-to-background ratio of approximately 5 % of what is found in the signal region and can therefore be used to estimate the background with low signal contamination.

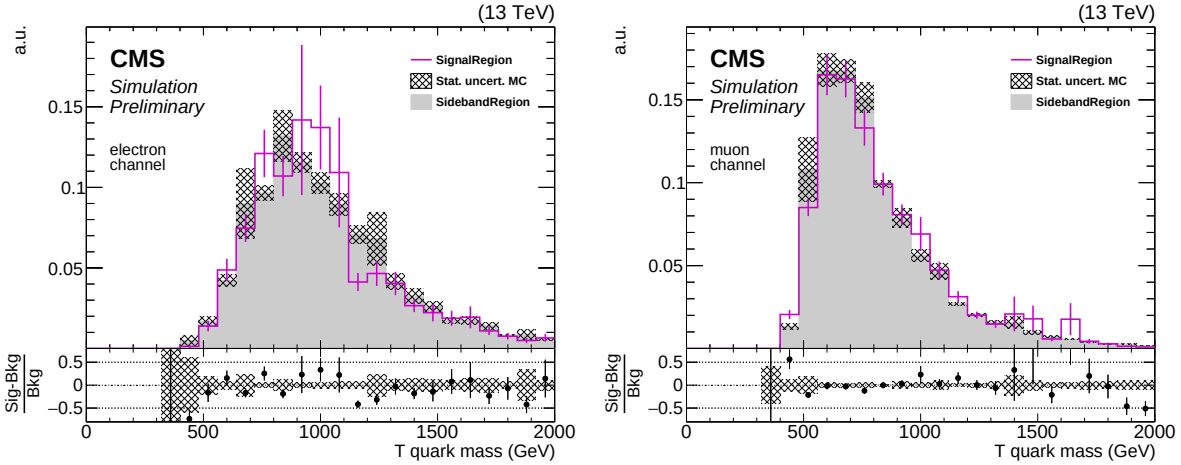

Figure 7: Comparison of vector-like T quark mass in the signal and sideband regions. The distributions show the sum of all background samples in the simulation. The electron channel is depicted on the left side and the muon channel on the right side.

The most important background processes contribute comparable relative fractions to the event yields in both regions. Both regions consist of 50—60 % top quark pair background and 20—30 % W + jets. A direct comparison of the T quark mass (M^{T}) in the sum of simulated background processes is shown in Fig. 7. We perform a χ^2 test [39] in order to evaluate the compatibility of the distributions and obtain p-values of 0.22 and 0.09 in the electron and muon channel, respectively. Therefore, the identity of the distributions can be accepted at 0.05 confidence level.

In the sideband region, 632 (2949) events of recorded data are selected in the electron (muon) channel. These relatively large numbers of events ensure that the statistical uncertainty is negligible compared to that in the signal region. In Fig. 8 the background estimate is shown alongside the distribution of M^{T} in the data.

7 Systematic uncertainties

Sources of systematic uncertainty may influence the rate and shape of the signal predictions as well as the shape of the background distribution. The statistical bin-by-bin uncertainty of the background estimate is taken into account as its shape uncertainty and its normalisation is not used in the following. For the signal simulation, we evaluate various rate and shape uncertainties. The largest uncertainty is introduced through the forward jet selection efficiency for the signal processes, followed by the b tag efficiency and jet energy correction uncertainties. The impacts of the systematic uncertainties on the event rates are listed in Tab. 3.

As b tagging requirements are applied in the signal and sideband region event selections, we employ b tag efficiency scale factors. Scale factors are applied to the simulations to reproduce the b tagging performance observed in data. The scale factors have a systematic uncertainty of 2—5 % for jets originating from b hadrons, 4—10% for c hadron jets and 7—10 % for light flavoured jets, all depending on the p_{T} of the jet. Those uncertainties are propagated to the end result, where the uncertainties of heavy flavour jets (b/c-hadrons) and light flavour jets

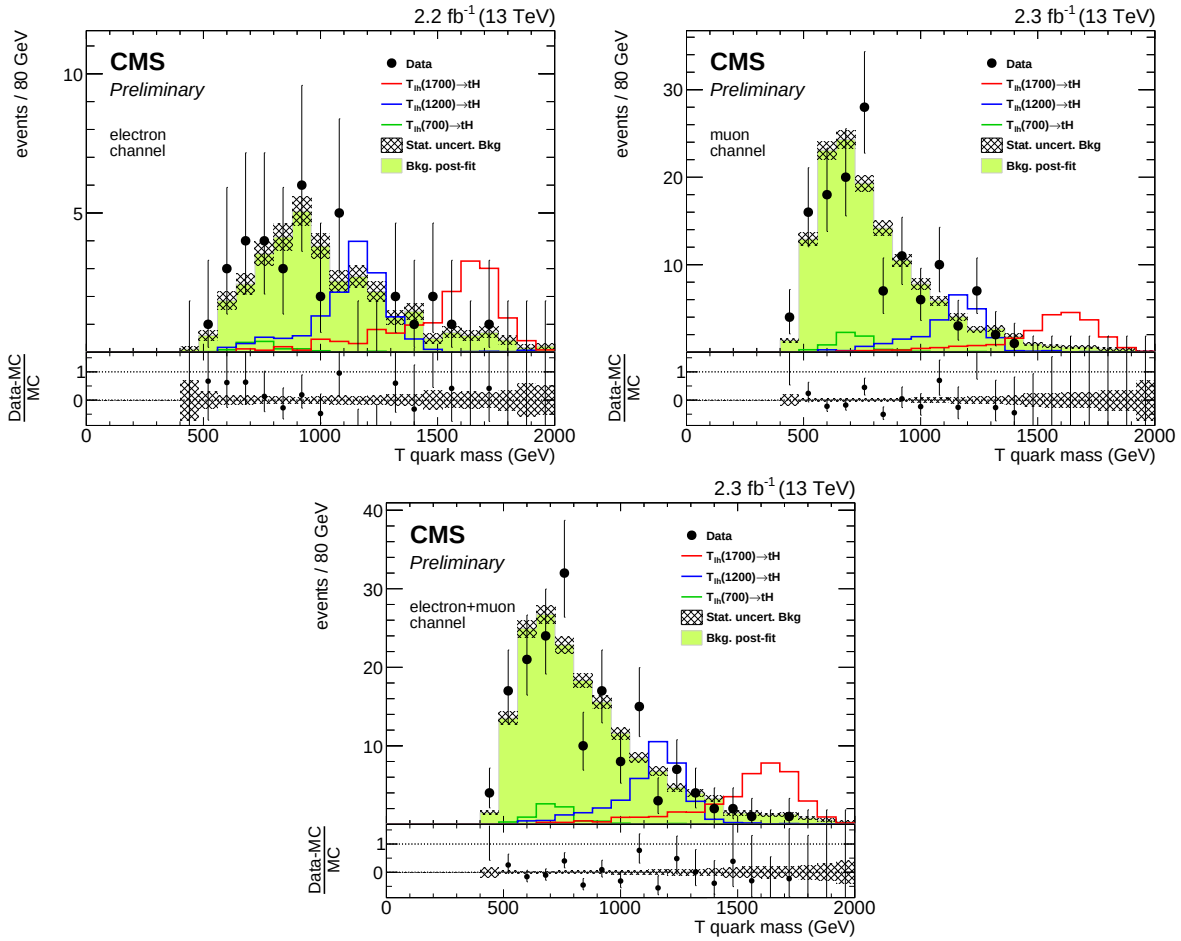

Figure 8: Distribution of M^{T}. The normalisation of the background estimate is shown as determined from the fit described in Sec. 8. The electron channel is found in the top left, the muon channel in the top right, and the sum of both channels is shown in the lower subfigure.

(u/d/s/g-hadrons) are treated as correlated within their group, but the uncertainties on heavy flavour jets are assumed to be uncorrelated with those on light jets.

Jet energy scale (JES) and resolution (JER) corrections are a function of the jet p_{T} and η. The associated uncertainties typically range on the order of a few percent. The resulting uncertainty is derived by applying the $\pm 1\sigma$ variations simultaneously to jets and AK8 jets and also propagating the variation of jet momenta into the calculation of $E_{\mathrm{T}}^{\mathrm{miss}}$ at the same time. Since the resolution of the jet p_{T} and soft-drop mass in the simulation is higher than in the data, these quantities receive a smearing in the simulation, and associated $\pm 1\sigma$ uncertainties are taken into account. Additionally, as the reconstruction efficiency of forward jets has been observed to be larger in the simulation as compared to the data, we assign a rate uncertainty of $\pm 15\%$ to the signal samples. This uncertainty is estimated by evaluating the forward jet selection efficiency in baseline-selected events that have exactly zero subjet b tags on the Higgs boson candidate.

For pileup, variations of $\pm 5\%$ of the minimum-bias cross-section are evaluated. Systematic identification and trigger uncertainties for electrons and muons are taken into account for the signal processes. For both trigger selection efficiencies, a conservative rate uncertainty of $\pm 5\%$ is assumed, which also covers for our lepton isolation requirement ($\Delta R(\ell, j)$ or $p_T^{\mathrm{rel}}(\ell, j)$). For the PDF uncertainty we evaluate the complete set of NNPDF 3.0 PDF eigenvectors, following the PDF4LHC prescription [40].

8 Exclusion Limits

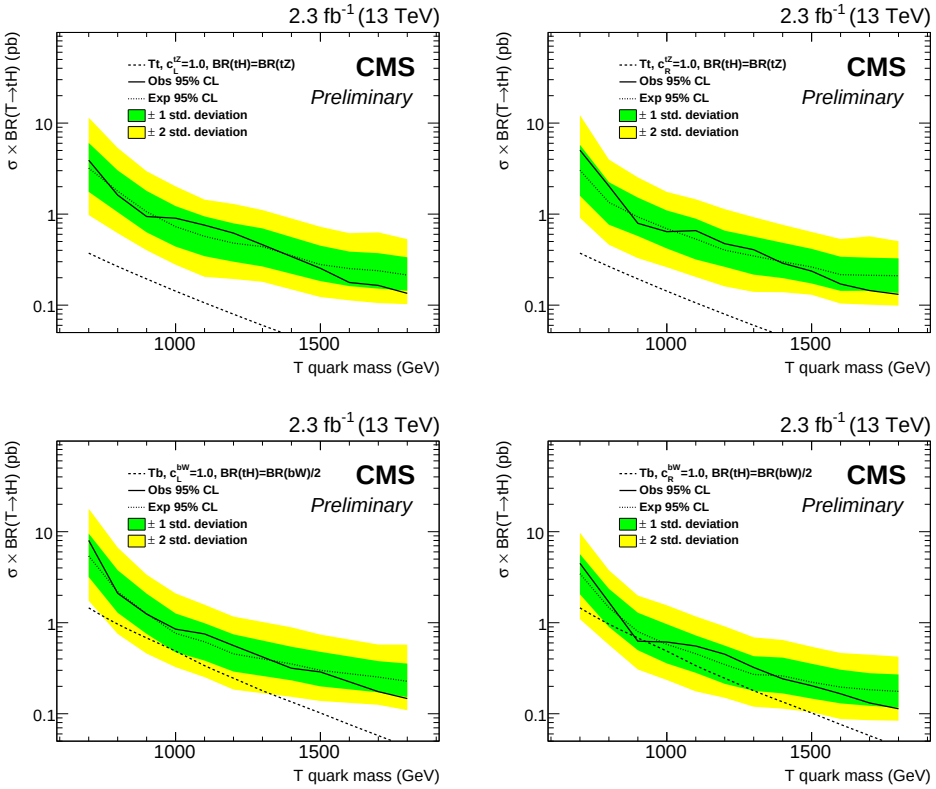

Figure 9: Exclusion limits on the cross section times branching ratio for left-handed and right-handed vector-like T quarks on the left and right side, respectively. Electron and muon channels are combined. Associated T production with a t (b) quark is shown in the two sub-figures at the top (bottom).

Table 3: Impacts of the largest systematic uncertainties on the signal event yields. Left-handed Tb production signal samples are shown. The uncertainties on the forward jet and lepton isolation and trigger are rate uncertainties, all other uncertainties are evaluated bin-by-bin. For the background estimate, the posterior uncertainty of the fit of a signal plus background model to the data distribution (Sec. 8) on the event rate is 12 %. All values are reported as percentages.

	electron channel			muon channel		
	T(0700)	T(1200)	T(1700)	T(0700)	T(1200)	T(1700)
forward jet	15.0	15.0	15.0	15.0	15.0	15.0
b tag heavy flav.	7.8	7.6	8.7	6.0	7.5	8.5
JES	8.9	4.9	4.9	3.0	5.7	4.6
lepton iso. and trg.	5.0	5.0	5.0	5.0	5.0	5.0

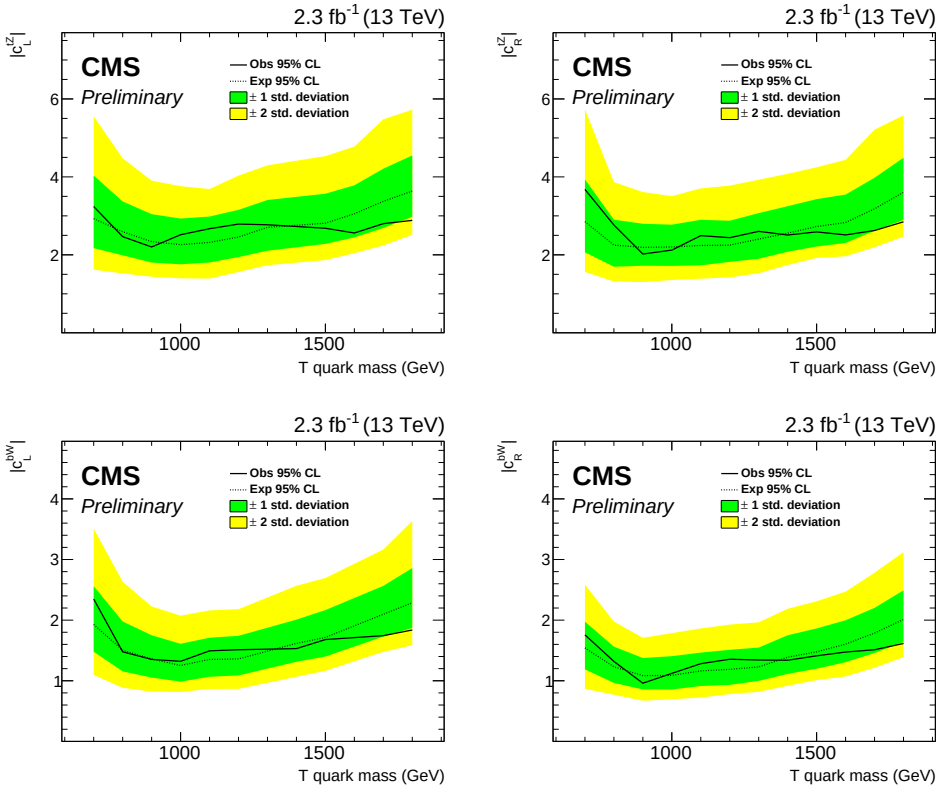

Figure 10: Coupling parameter exclusion limits for left-handed and right-handed vector-like T quarks on the left and right side, respectively. Electron and muon channels are combined. Associated T production with a t (b) quark is shown in the two sub-figures at the top (bottom).

No significant excess over the expected standard model event yields is observed. We set exclusion limits on the production cross section times branching ratio for a single vector-like T quark decaying to a top quark and a Higgs boson. The 95 % confidence level (CL) exclusion limits are derived with a Bayesian statistical method [41, 42], where background and signal templates in the M^{T} distribution are fitted to the data with a combined fit in the electron and muon channels. Systematic uncertainties are included as nuisance parameters. For rate-only uncertainties we assign a log-normal prior and a flat prior is used for the signal strength as well as the background distribution. Template morphing with cubic-linear interpolation is used to deal with shape uncertainties. The statistical uncertainty of the background estimate is included with the 'Barlow-Beeston light' method [43], using a Gaussian approximation of the uncertainty in each bin.

We compare the exclusion limits obtained with predictions from two benchmark models. For Tb production, a branching fraction scenario of 50/25/25 % for the T quark decay to bW/tZ/tH is considered. A scenario with neutral currents only and equal couplings to tZ and tH is used for Tt production (0/50/50 %). Signal cross sections are taken from NLO calculations [44, 45] and multiplied with a factor of 0.25 and 0.5 in order to accommodate the branching ratio BR(tH)=BR(bW)/2 and BR(tH)=BR(tZ) for Tb and Tt production, respectively. A coupling strength of $c_{\mathrm{L/R}} = 1$ is assumed in production.

Figure 9 shows the 95 % CL upper limits on the cross section times branching ratios, along with the predictions from the benchmark models. The results are further interpreted as exclusion limits on the T quark coupling constants as a function of mass as shown in Fig. 10.

9 Summary

A search for a vector-like T quark decaying to top quark and Higgs boson is presented, where the top quark decay involves an electron or muon and the Higgs boson decays into a pair of b quarks. For every event, a four momentum of the potential vector-like T quark is reconstructed and its mass is evaluated. No excess over the estimated backgrounds is observed and 95 % CL upper limits are placed on the cross section times branching ratio for vector-like T quarks and its coupling to third generation standard model quarks in the mass range of 700 GeV to 1800 GeV. Complementing the pair production searches for vector-like T quarks, this is the first analysis setting exclusion limits on the cross section and coupling parameters of singly produced vector-like T quarks at a centre-of-mass energy of 13 TeV.

References

[1] N. Arkani-Hamed, A. G. Cohen, and H. Georgi, "Electroweak symmetry breaking from dimensional deconstruction", *Phys. Lett. B* **513** (2001) 232, doi:10.1016/S0370-2693(01)00741-9, arXiv:hep-ph/0105239.

[2] M. Schmaltz and D. Tucker-Smith, "Little Higgs review", *Ann. Rev. Nucl. Part. Sci.* **55** (2005) 229, doi:10.1146/annurev.nucl.55.090704.151502, arXiv:hep-ph/0502182.

[3] I. Antoniadis, K. Benakli, and M. Quiros, "Finite Higgs mass without supersymmetry", *New J. Phys.* **3** (2001) 20, doi:10.1088/1367-2630/3/1/320, arXiv:hep-th/0108005.

[4] Y. Hosotani, S. Noda, and K. Takenaga, "Dynamical gauge-Higgs unification in the electroweak theory", *Phys. Lett. B* **607** (2005) 276, doi:10.1016/j.physletb.2004.12.029, arXiv:hep-ph/0410193.

[5] K. Agashe, R. Contino, and A. Pomarol, "The minimal composite Higgs model", *Nucl. Phys. B* **719** (2005) 165, doi:10.1016/j.nuclphysb.2005.04.035, arXiv:hep-ph/0412089.

[6] ATLAS Collaboration, "Observation of a new particle in the search for the Standard Model Higgs boson with the ATLAS detector at the LHC", *Phys. Lett. B* **716** (2012) 1, doi:10.1016/j.physletb.2012.08.020, arXiv:1207.7214.

[7] CMS Collaboration, "Observation of a new boson at a mass of 125 GeV with the CMS experiment at the LHC", *Phys. Lett. B* **716** (2012) 30, doi:10.1016/j.physletb.2012.08.021, arXiv:1207.7235.

[8] CMS Collaboration, "Observation of a new boson with mass near 125 GeV in pp collisions at $\sqrt{s}$ = 7 and 8 TeV", *JHEP* **06** (2013) 081, doi:10.1007/JHEP06(2013)081, arXiv:1303.4571.

[9] O. Eberhardt et al., "Joint analysis of Higgs boson decays and electroweak precision observables in the standard model with a sequential fourth generation", *Phys. Rev. D* **86** (2012) 013011, doi:10.1103/PhysRevD.86.013011, arXiv:1204.3872.

[10] J. A. Aguilar-Saavedra, R. Benbrik, S. Heinemeyer, and M. Pérez-Victoria, "Handbook of vector-like quarks: mixing and single production", *Phys. Rev. D* **88** (2013) 094010, doi:10.1103/PhysRevD.88.094010, arXiv:1306.0572.

[11] CMS Collaboration, "Search for Vectorlike Charge 2/3 T Quarks in Proton-Proton Collisions at $\sqrt{s}$ = 8 TeV", *Phys. Rev. D* **93** (2016) 012003, doi:10.1103/PhysRevD.93.012003, arXiv:1509.04177.

[12] ATLAS Collaboration, "Search for pair and single production of new heavy quarks that decay to a Z boson and a third-generation quark in pp collisions at $\sqrt{s} = 8$ TeV with the ATLAS detector", *JHEP* **11** (2014) 104, doi:10.1007/JHEP11(2014)104, arXiv:1409.5500.

[13] ATLAS Collaboration, "Analysis of events with b-jets and a pair of leptons of the same charge in pp collisions at $\sqrt{s} = 8$ TeV with the ATLAS detector", (2015). arXiv:1504.04605. Accepted by *JHEP* (2015).

[14] ATLAS Collaboration, "Search for production of vector-like quark pairs and of four top quarks in the lepton-plus-jets final state in pp collisions at $\sqrt{s} = 8$ TeV with the ATLAS detector", *JHEP* **08** (2015) 105, doi:10.1007/JHEP08(2015)105, arXiv:1505.04306.

[15] CMS Collaboration, "Search for vector-like T quarks decaying to top quarks and Higgs bosons in the all-hadronic channel using jet substructure", *JHEP* **06** (2015) 080, doi:10.1007/JHEP06(2015)080, arXiv:1503.01952.

[16] CMS Collaboration, "The CMS experiment at the CERN LHC", *JINST* **3** (2008) S08004, doi:10.1088/1748-0221/3/08/S08004.

[17] CMS Collaboration, "Particle-flow event reconstruction in CMS and performance for jets, taus, and $E_{\mathrm{T}}^{\mathrm{miss}}$", CMS Physics Analysis Summary CMS-PAS-PFT-09-001, 2009.

[18] CMS Collaboration, "Commissioning of the particle-flow event with the first LHC collisions recorded in the CMS detector", CMS Physics Analysis Summary CMS-PAS-PFT-10-001, 2010.

[19] CMS Collaboration, "Performance of electron reconstruction and selection with the CMS detector in proton-proton collisions at $\sqrt{s} = 8\,\text{TeV}$", *JINST* **10** (2015) P06005, doi:10.1088/1748-0221/10/06/P06005, arXiv:1502.02701.

[20] CMS Collaboration, "Performance of CMS muon reconstruction in pp collision events at $\sqrt{s} = 7\,\text{TeV}$", *JINST* **7** (2012) P10002, doi:10.1088/1748-0221/7/10/P10002, arXiv:1206.4071.

[21] M. Cacciari, G. P. Salam, and G. Soyez, "The anti-k_t jet clustering algorithm", *JHEP* **04** (2008) 063, doi:10.1088/1126-6708/2008/04/063, arXiv:0802.1189.

[22] M. Cacciari, G. P. Salam, and G. Soyez, "FastJet user manual", *Eur. Phys. J. C* **72** (2012) 1896, doi:10.1140/epjc/s10052-012-1896-2, arXiv:1111.6097.

[23] M. Cacciari, G. P. Salam, and G. Soyez, "The catchment area of jets", *JHEP* **04** (2008) 005, doi:10.1088/1126-6708/2008/04/005, arXiv:0802.1188.

[24] CMS Collaboration Collaboration, "Determination of jet energy calibration and transverse momentum resolution in CMS", *JINST* **6** (2011) P11002, doi:10.1088/1748-0221/6/11/P11002, arXiv:1107.4277.

[25] P. Nason, "A New method for combining NLO QCD with shower Monte Carlo algorithms", *JHEP* **11** (2004) 040, doi:10.1088/1126-6708/2004/11/040, arXiv:hep-ph/0409146.

[26] S. Frixione, P. Nason, and C. Oleari, "Matching NLO QCD computations with Parton Shower simulations: the POWHEG method", *JHEP* **11** (2007) 070, doi:10.1088/1126-6708/2007/11/070, arXiv:0709.2092.

[27] S. Alioli, P. Nason, C. Oleari, and E. Re, "A general framework for implementing NLO calculations in shower Monte Carlo programs: the POWHEG BOX", *JHEP* **06** (2010) 043, doi:10.1007/JHEP06(2010)043, arXiv:1002.2581.

[28] S. Frixione, P. Nason, and G. Ridolfi, "A Positive-weight next-to-leading-order Monte Carlo for heavy flavour hadroproduction", *JHEP* **09** (2007) 126, doi:10.1088/1126-6708/2007/09/126, arXiv:0707.3088.

[29] E. Re, "Single-top Wt-channel production matched with parton showers using the POWHEG method", *Eur. Phys. J. C* **71** (2011) 1547, doi:10.1140/epjc/s10052-011-1547-z, arXiv:1009.2450.

[30] J. Alwall et al., "The automated computation of tree-level and next-to-leading order differential cross sections, and their matching to parton shower simulations", *JHEP* **07** (2014) 079, doi:10.1007/JHEP07(2014)079, arXiv:1405.0301.

[31] M. L. Mangano, M. Moretti, F. Piccinini, and M. Treccani, "Matching Matrix Elements and Shower Evolution for Top-Quark Production in Hadronic Collisions", *JHEP* **01** (2007) 013, doi:10.1088/1126-6708/2007/01/013, arXiv:hep-ph/0611129.

[32] Sjöstrand, Torbjörn and Mrenna, Stephen and Skands, Peter Z., "PYTHIA 6.4 Physics and Manual", *JHEP* **05** (2006) 026, doi:10.1088/1126-6708/2006/05/026, arXiv:hep-ph/0603175.

[33] T. Sjöstrand et al., "An Introduction to PYTHIA 8.2", *Comput. Phys. Commun.* **191** (2015) 159–177, doi:10.1016/j.cpc.2015.01.024, arXiv:1410.3012.

[34] NNPDF Collaboration, "Parton distributions for the LHC Run II", *JHEP* **04** (2015) 040, doi:10.1007/JHEP04(2015)040, arXiv:1410.8849.

[35] CMS Collaboration, "Description and performance of track and primary-vertex reconstruction with the CMS tracker", *JINST* **9** (2014) P10009, doi:10.1088/1748-0221/9/10/P10009, arXiv:1405.6569.

[36] W. Waltenberger, R. Früwirth, and P. Vanlaer, "Adaptive Vertex Fitting", *J. Phys. G: Nucl. Part. Phys.* **34** (2007) N343, doi:10.1088/0954-3899/34/12/N01.

[37] CMS Collaboration, "Identification of b-quark jets with the CMS experiment", *JINST* **8** (2013) P04013, doi:10.1088/1748-0221/8/04/P04013, arXiv:1211.4462.

[38] A. J. Larkoski, S. Marzani, G. Soyez, and J. Thaler, "Soft Drop", *JHEP* **05** (2014) 146, doi:10.1007/JHEP05(2014)146, arXiv:1402.2657.

[39] N. D. Gagunashvili, "Comparison of weighted and unweighted histograms", arXiv:physics/0605123.

[40] J. Butterworth et al., "PDF4LHC recommendations for LHC Run II", *J. Phys. G: Nucl. Part. Phys.* **43** (2016) 023001, doi:10.1088/0954-3899/43/2/023001.

[41] T. Müller, J. Ott, and J. Wagner-Kuhr, "theta - a framework for template-based modeling and inference",. http://www-ekp.physik.uni-karlsruhe.de/~ott/theta/testing/html/theta__auto__intro.html.

[42] A. O'Hagan and J. J. Forster, "Kendall's Advanced Theory of Statistics. Vol. 2B: Bayesian Inference". Arnold, London, 2004.

[43] R. J. Barlow and C. Beeston, "Fitting using finite Monte Carlo samples", *Comput.Phys.Commun.* **77** (1993) 219, doi:10.1016/0010-4655(93)90005-W.

[44] O. Matsedonskyi, G. Panico, and A. Wulzer, "On the interpretation of Top Partners searches", *Journal of High Energy Physics* **2014** (2014) 1–34, doi:10.1007/JHEP12(2014)097.

[45] J. Campbell, R. K. Ellis, and F. Tramontano, "Single top-quark production and decay at next-to-leading order", *Phys. Rev. D* **70** (Nov, 2004) 094012, doi:10.1103/PhysRevD.70.094012.